A&A 486, 311–323 (2008)
DOI: 10.1051/0004-6361:20078421

Astronomy & Astrophysics

Spectral irradiance variations: comparison between observations and the SATIRE model on solar rotation time scales

Y. C. Unruh[1], N. A. Krivova[2], S. K. Solanki[2], J. W. Harder[3], and G. Kopp[3]

[1] Astrophysics Group, Blackett Laboratory, Imperial College London, SW7 2AZ, UK
e-mail: y.unruh@imperial.ac.uk
[2] Max-Planck-Institut für Sonnensystemforschung, 37191 Katlenburg-Lindau, Germany
[3] Laboratory for Atmospheric and Space Physics, 1234 Innovation Drive, Boulder, Colorado 80303-7814, USA

Received 4 August 2007 / Accepted 27 February 2008

ABSTRACT

Aims. We test the reliability of the observed and calculated spectral irradiance variations between 200 and 1600 nm over a time span of three solar rotations in 2004.
Methods. We compare our model calculations to spectral irradiance observations taken with SORCE/SIM, SoHO/VIRGO, and UARS/SUSIM. The calculations assume LTE and are based on the SATIRE (Spectral And Total Irradiance REconstruction) model. We analyse the variability as a function of wavelength and present time series in a number of selected wavelength regions covering the UV to the NIR. We also show the facular and spot contributions to the total calculated variability.
Results. In most wavelength regions, the variability agrees well between all sets of observations and the model calculations. The model does particularly well between 400 and 1300 nm, but fails below 220 nm, as well as for some of the strong NUV lines. Our calculations clearly show the shift from faculae-dominated variability in the NUV to spot-dominated variability above approximately 400 nm. We also discuss some of the remaining problems, such as the low sensitivity of SUSIM and SORCE for wavelengths between approximately 310 and 350 nm, where currently the model calculations still provide the best estimates of solar variability.

Key words. Sun: activity – Sun: faculae, plages – Sun: sunspots – Sun: photosphere

1. Introduction

The solar irradiance, or the solar flux received at the top of the Earth's atmosphere, is known to vary over a large number of time scales, ranging from minutes to months and decades. The changes in the total solar output have been measured since 1978 (Willson & Hudson 1988) and different composites of the measurements have been presented by Fröhlich & Lean (1998); Willson & Mordvinov (2003) and Dewitte et al. (2004). While the short-term (minutes to hour) variability is mainly due to solar oscillations and granulation, the daily to decadal variability is attributed to the changes in the surface magnetic field combined with the solar rotation that transports solar active regions into and out of view. Indeed, Krivova et al. (2003) found that more than 90% of the solar variability between 1996 and 2002 could be explained by changes in the solar surface field. Similar conclusions were reached by Wenzler et al. (2006) who reconstructed solar irradiance from Kitt Peak magnetograms covering the last 3 solar cycles.

Solar variability is a strong function of wavelength: while solar output is small in the UV, the relative variability is more than one order of magnitude larger in the UV than in the visible. Until very recently, the spectral dependence of the solar variability had mainly been determined in the UV, in particular by the measurements taken by the SUSIM and SOLSTICE instruments onboard UARS (see, e.g., Floyd et al. 2003a). Information in the visible was restricted to the three colour channels of the SPM instrument of SOHO/VIRGO (Fröhlich et al. 1995), though degradation hampered the use of these data beyond timescales of the order of a few months[1].

The variability at most other wavelengths had to be inferred using a variety of approaches, such as e.g., pioneered by Lean (1989) who produced the first estimate of solar-cycle variability over a large wavelength range. An alternative approach was followed by Unruh et al. (1999) who used facular and spot model atmospheres to calculate the flux changes due to magnetic features. Fligge et al. (2000) and Krivova et al. (2003) used solar surface images and magnetograms to calculate the variability on time scales ranging from days to years. Here we built on this approach and present comparisons between modelled and measured spectral irradiances during three months in 2004.

Thanks to missions such as SORCE and SCIAMACHY the observational outlook has now become much better and we have, for the first time, variability observations that span from the UV to the near IR (Harder et al. 2005b; Rottman et al. 2005; Skupin et al. 2005). In the following we consider SORCE data only. First comparisons between SORCE measurements and models have been presented by, e.g., Fontenla et al. (2004) and Lean et al. (2005).

All data presented here have been recorded between 21 April and 1 August 2004. During this time the Sun was in a relatively quiet phase, especially in May when only a very small

[1] SPM data are available from ftp://ftp.pmodwrc.ch/pub/data/irradiance/virgo/SSI/spm_level2_d_170496_06.dat; see also ftp://ftp.pmodwrc.ch/pub/Claus/SORCE_Sep2006/SSI_Poster.pdf

spot group appeared on the solar disk. A new and larger active region emerged over the next month, resulting in a depression of just over 1 permille in total solar irradiance (TSI) in July.

In the next section we briefly describe our irradiance modelling approach. We then discuss the data analysis for the different instruments (Sect. 3). In Sect. 4, we compare the relative irradiance changes derived from the models with a number of different data sets spanning a wavelength range from 200 to 1600 nm. In particular, we compare our model to data from SORCE/SIM, UARS/SUSIM, and SoHO/VIRGO. We conclude this section by presenting observed and modelled timeseries in a number of selected wavelength bands. A discussion of the results and conclusions are presented in Sect. 5.

2. Irradiance reconstructions

Here we restrict ourselves to a brief description of our approach to model solar irradiance (see Fligge et al. 2000; Krivova et al. 2003, for a more detailed discussion). Essentially, we calculate the solar irradiance (or flux) by integrating over the (pixellated) solar surface, accounting for the presence of dark (sunspots) and bright (faculae and network) surface magnetic features. The location of sunspots is obtained from MDI continuum images, attributing penumbra and umbra to those pixels with contrasts of less than 0.9 and 0.6, respectively. Faculae and the network are identified by their excess magnetic flux on MDI magnetograms. As faculae are very small-scale features and typically do not fill an entire MDI pixel, we adopt a filling-factor approach, scaling the facular filling factor (linearly) with the magnetic field strength measured from the magnetograms. The identification of the magnetic features is described more extensively in Fligge et al. (2000) and Krivova et al. (2003).

The model has a single free parameter, $B_{\rm sat}$, which takes into account the saturation of brightness in regions with higher concentration of magnetic elements (e.g., Solanki & Stenflo 1984; Solanki & Brigljević 1992; Ortiz et al. 2002). $B_{\rm sat}$ denotes the field strength below which the facular contrast is proportional to the magnetogram signal, while it is independent (saturated) above that. From a fit to the VIRGO TSI time series Krivova et al. (2003) obtained a value of 280 G for $B_{\rm sat}$, which is used here unchanged.

Once each pixel on the solar surface has been identified as either (part) facula, quiet Sun, umbra or penumbra, we can attribute a corresponding emergent intensity to it and then proceed to carry out the disk integration. Note that the emergent intensities have to be known as a function of limb angle for each of the components present on the solar surface. The wavelength resolution and available range for the final spectral irradiance is determined by the wavelength resolution and range of the limb-dependent emergent intensities.

We calculate the intensities from the SATIRE set of model atmospheres (Unruh et al. 1999), using Kurucz's ATLAS9 program (Kurucz 1993). The model atmosphere for the faculae and network was derived using FAL P (Fontenla et al. 1999) as a starting point, while the quiet-sun is Kurucz's standard solar atmosphere and the sunspot umbra and penumbra models are stellar models at 4500 K and 5150 K also taken from Kurucz (1993). As the model atmospheres and intensities are derived under the assumption of LTE, we expect our irradiances to become unreliable below approximately 300 nm (see, e.g., Unruh et al. 1999; Krivova et al. 2006).

For the comparisons presented in this paper, the availability of MDI images[2] and groups of five consecutive magnetograms (which were averaged to reduce the noise) was reasonably good and we were mostly able to calculate irradiances on a 12-hourly interval. There are, however, some data gaps, most noticeably at the end of June with only three sets of images with poorer quality between 2004 June 22 and June 30.

3. Solar irradiance observations: May to July 2004

The main instruments used for the comparisons are the spectral and total irradiance monitors from SORCE, SIM and TIM, respectively. These data are complemented by contemporaneous observations from UARS/SUSIM and VIRGO/SPM. In this section, we briefly describe the instruments used and discuss the data analysis.

SORCE (Solar Radiation and Climate Experiment) was launched in January 2003 and started science operations in March of that year. It is the first satellite to provide reliable daily measurements of the spectral irradiance variability for wavelengths longer than 400 nm. It carries four instruments, all of which have been described in Rottman et al. (2005) and sources referenced therein.

3.1. SORCE/SIM

SIM primarily measures spectral irradiance between 300 and 2400 nm with an additional channel to cover the 200 to 300 nm wavelength region. We consider data taken with three of its five detectors, namely the UV detector (200–308 nm), the VIS1 detector (VIS1: 310–1000 nm), and the IR detector (994–1655 nm). These will be discussed briefly in the following sections. We discard the data from the second visible-light detector as it suffers from both temperature and radiation-induced variability that cannot be fully removed. We were unable to use the longer-wavelength data recorded by SIM/ESR as they were too noisy over the time span considered here. For more information on the design and calibration of SIM we refer to Harder et al. (2005a,b).

The results presented here are based on Version 10 of the SIM data reduction. The availability of SORCE data in the time considered here is reasonably good with only some data gaps and correction problems during two weeks around the end of June and beginning of July. The SOHO/MDI suffered from poorer imaging data during these two weeks as well, making comparisons at these times more difficult.

All three detectors provide measurements of the solar irradiance as a function of wavelength on approximately 12-h intervals. As discussed in Harder et al. (2005b), SIM typically has 6 samples per resolution element, yielding an (un-aliased) oversampling by about a factor of 2. In order to compare the data to the model calculations, we characterise them in two ways. Firstly, we consider the variability, treating each wavelength bin as an independent time series. As a measure of the variability, we adopt the standard deviation, calculated according to

$$\sigma(\lambda_i) = \sqrt{\frac{\sum_{j=1}^{n} \left(f_j(\lambda_i) - \bar{f}(\lambda_i)\right)^2}{(n-1)}}, \quad (1)$$

where $\bar{f}(\lambda_i)$ is the mean flux at wavelength λ_i and $f_j(\lambda_i)$ is the flux at time j and wavelength λ_i. So as to better illustrate the

[2] All MDI images were obtained from the MDI homepage at http://soi.stanford.edu/

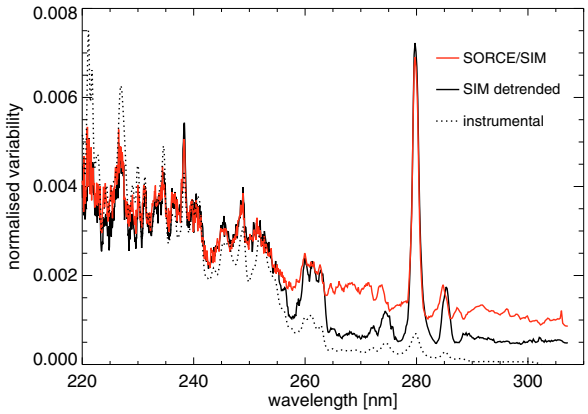

Fig. 1. The normalised standard deviation between 220 and 310 nm as derived from SIM/UV between 2004 April 21 and August 1. The red and black lines show the normalised standard deviation of the smoothed data after the removal of outliers. The difference between the two variability spectra is due to the removal of a linear slope that reduces the variability for wavelengths above about 260 nm as indicated by the black line (see Sect. 3.1). The dotted line traces the instrumental noise. Note that the instrumental noise exceeds the binomially smoothed signal for wavelengths below approximately 230 nm.

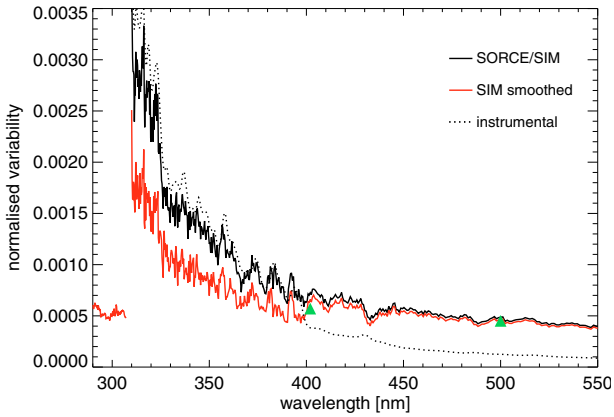

Fig. 2. Variability between 2004 April 21 and Aug. 1 as recorded with the SIM/VIS1 instrument. The black line shows the normalised deviation of the Version 10 data after the removal of outliers. The red line is for the variability of binomially smoothed data, while the dotted line indicates the instrumental noise. Also shown is the variability measured in the VIRGO blue and green filters (green triangles). The short data stretch below 308 nm is as measured with SIM/UV.

relative changes in each wavelength bin, we only plot the *normalised* standard deviation, i.e., $\sigma(\lambda_i)/\bar{f}(\lambda_i)$. This measure has the advantage of simplicity and universality, but has the disadvantage that it makes disentangling facular and spot variability difficult. Secondly, we look at time series in a number of selected wavelength bins. These include the VIRGO/SPM filter bands, which allow us to compare our model, SORCE/SIM and VIRGO/SPM with each other, and a number of bands that stand out in the variability plots.

Before calculating the final rms spectra, the mean spectra and the time series, we removed obvious outliers in the SIM data. This was done for each wavelength bin individually, by removing data points that deviated from the mean by more than $k\sigma$. The cutoff factor, k, was varied with wavelength to account for the different aspects of the faculae-dominated variability in the UV and the spot-dominated variability at longer wavelengths. We thus applied a symmetric cutoff in the UV, generally clipping data points more than 3.5σ from the mean. In the visible and infrared, typically data points more than 2σ above and 4.5σ below the mean were clipped. The clipped data were replaced by median values of the two previous and subsequent exposures.

The variability plots are shown in Figs. 1 and 2 and will be discussed in the following sections. The plots also show the derived instrumental noise level. Note that SIM is generally not photon-noise limited, but analog-to-digital converter (ADC) limited with about 2 bits of noise on a 15-bit converter range. It requires a dynamic range of aproximately 100 to measure the signal, so for weak signals the noise level becomes comparable to the solar variability signature. Apart from these random noise contributions, additional residual systematic trends caused by the imperfect prism degradation and temperature corrections can still be present in the time series. As the analog-to-digital noise is essentially random, the application of a (non-phase shifting) filter is appropriate. Here we use binomial smoothing (Marchand & Marmet 1983) in the time domain with two passes of the lowest-order (1,2,1) filter, meaning that we will be insensitive to variability on time scales shorter than about 1.5 days.

3.1.1. SIM/UV

Solar variability is very much higher in the UV than in the visible and infrared, and robust measurements with variations of the order of several percent are expected. Harder et al. (2005b) have shown that the response of the UV instrument becomes more unreliable towards the blue end of the wavelength range. Figure 1 shows the normalised standard deviation for the SIM/UV data. The red line indicates the normalised standard deviation of the original Version 10 data set, once outliers have been removed. The black dotted line indicates the instrumental noise.

Over the time span considered here, the data from the UV detector show a slow, almost linear, decrease that introduces substantial variability and can be picked up in the 264 to 277 nm and 290 to 300 nm regions in particular. This decrease could be either instrumental or instrinsically solar in which case it would imply a slow decrease of the normalised solar UV irradiance at the 5000 ppm level over a 3-month time span. A solar origin is supported by a comparison to the SORCE/SOLSTICE instrument (Snow et al. 2005) over the same time span. While the SOLSTICE trend deviates in the first couple of weeks, it generally agrees with the SIM measurements for the remainder of the time. The red line in Fig. 1 shows the normalised standard deviation when the linear trend is removed. In this case, the variability around 270 nm decreases by a factor of 2 in better agreement with what is seen in the models (see Sect. 4.4).

The measured standard deviation agrees well between the smoothed and unsmoothed data for wavelengths larger than approximately 260 nm where it also exceeds the instrumental noise by more than a factor of two. For wavelengths below 240 nm the instrumental noise becomes comparable to the data variability. This indicates that the measured variability is largely instrumental on the roughly 12-hourly timescales considered here, and can thus be significantly reduced by binomial smoothing as applied here. Indeed, for wavelengths below 235 nm, the variability of the smoothed data falls below the instrumental noise.

3.1.2. SIM/VIS1

Figure 2 shows the variability measured with VIS1 for wavelengths between 310 and 550 nm. The red and black lines show the smoothed and unsmoothed data, respectively. Also shown is the instrumental noise level (dotted line). The figure illustrates that the instrumental variability increases dramatically for wavelengths shortward of approximately 400 nm (see also Fig. 2 in Woods 2007). While there is no marked difference between the smoothed and unsmoothed data above 400 nm, indicating that we measure a predominantly solar signal, the variability of the smoothed data is lower (by a factor of about 1.5) at shorter wavelengths and falls below the instrumental noise level. It is thus not straightforward to estimate the solar variability from the data available here, or indeed even estimate unambiguously the range up to which the smoothed data represent solar rather than instrumental signal.

Overall, an increase in the standard deviation is expected for lower wavelengths, though the variability seen between 310 and 350 nm is clearly too high. We can take some guidance from the standard deviation of 500 ppm recorded with the SIM/UV detector at 300 nm. We would, however, caution against interpolating the variability between 300 and 390 nm, despite the similar variability levels observed at both wavelengths. Not only does the region contain a number of intermediate-strength lines, it also coincides with the expected switch-over between the facular and spot-dominated regime on rotational time scales. Depending on the exact balance between facular brightening and sunspot darkening, both effects can almost cancel each other out. This would explain, e.g., why the variability is lower at 385 and 395 nm compared to 400 nm.

Not shown in Fig. 2 is the VIS1 variability above 550 nm, as it is mainly featureless: it shows a slow decrease between 550 nm to 800 nm where it ranges from 350 ppm down to about 270 ppm. For longer wavelengths (>820 nm) it shows an upturn. This variability increase was already noted by Harder et al. (2005b) who attributed it to the incomplete removal of temperature-induced variability in the instrument. The variability recorded by SIM/VIS1 is shown over the full wavelength range and discussed further in Sect. 4.4 where it is compared to the model results.

3.1.3. SIM/IR

SIM/IR, the infrared detector records the solar spectrum between 850 nm and 1.66 μm. The data in the IR suffer from occasional sudden data jumps in time. The data become particularly noisy at the detector edges. We thus only use data for wavelengths between 980 and 1600 nm in the following. In this wavelength range, the data are very uniform with a normalised standard deviation between 230 and 300 ppm.

3.2. SORCE/TIM

With TIM, the Total Irradiance Monitor, the SORCE satellite also carries a solar radiometer to measure total solar irradiance. The TIM instrument has been described in detail by Kopp & Lawrence (2005) and first results have been presented in Kopp et al. (2005). The instrumental noise level is less than 2 ppm and the instrumental stability is corrected to <10 ppm/yr, so the TIM data require no long-term gradient removal or high-frequency temporal filtering for the analyses here using Version 5 data. The TSI measured by SORCE/TIM is about 5 W m^{-2} lower than the TSI measured by other radiometers in space, such as, ACRIM-III and VIRGO (Fröhlich et al. 1997). The irradiance changes of TIM, however, agree extremely well with those of the other radiometers, not only over the three months considered here, but also over the whole life time of the SORCE mission. Here we use TIM as representative for the TSI. As we consider relative changes in TSI only, we have normalised the modelled and SIM-integrated data (see Sect. 4.1) to the SORCE/TIM values.

3.3. UARS/SUSIM

The Solar Ultraviolet Spectral Irradiance Monitor (SUSIM) is a dual dispersion spectrometer instrument that operated from 1991 to 2005 (Brueckner et al. 1993). It was one of the 2 UV experiments on board UARS (Upper Atmosphere Research Satellite). SUSIM has been monitoring solar irradiance in the range from 115 to 410 nm with a spectral resolution between 0.15 and 5 nm. We use the daily level 3BS V22 data with sampling of 1 nm (Floyd et al. 2003b, Floyd, priv. comm. 2006) available at `ftp://ftp.susim.nrl.navy.mil`. Calibration of the changing responsivity of SUSIM's working channel was done through a combination of measurements of four on-board deuterium calibration lamps and solar measurements by less frequently exposed reference optical channels (Prinz et al. 1996; Floyd et al. 1998). The long-term uncertainty of irradiance measurements (1σ) is about 2–3% at $\lambda > 170$ nm, ≈5% at $\lambda = 140$–170 nm and increases to around 10–20% at shorter wavelengths (Woods et al. 1996; Floyd et al. 1998, 2003b).

3.4. VIRGO

The VIRGO/SPM instrument onboard SOHO measures solar variability in three wavelength bands, centred on 402 (blue), 500 (green) and 862 nm (red) with bandwidths (*FWHM*) of 5.4, 5.0 and 5.7 nm, respectively. The data presented here are level 1.7 daily averages and have been obtained from the SOHO data archive. SPM measurements suffer from strong and non-linear degradation, so that stretches longer than one month need to be corrected carefully before they can be used for comparison purposes. To correct for the degradation, we divided the VIRGO/SPM data by VIRGO TSI data and fitted a quadratic function to 9 data points that coincide with times of low solar activity. This essentially pins the long-term behaviour in the colour channels to that of the TSI during quiet-Sun phases.

Note that a newer SPM data release has recently become available where most of the long-term degradation has been removed (Fröhlich 2007, priv. comm). A comparison between our corrected data with the new data release shows that the variability amplitudes agree very well. A small amount of (possibly spurious) long-term variability, however, remains even in the new data set. Rather than carrying out a similar procedure as outlined above, we decided to use the old, but corrected data set.

4. Comparisons of the SATIRE model to SORCE/SIM and SOHO/VIRGO measurements

4.1. Total solar irradiance

As a first test, we compare the modelled total solar irradiance to the SORCE/TIM measurements as well as to the SORCE/SIM "total" solar irradiance. This SIM pseudo-TSI was obtained by integrating the (smoothed) SORCE/SIM measurements over the available SIM wavelength range. As this does not cover the full solar spectrum, the resulting integrated irradiance is, at

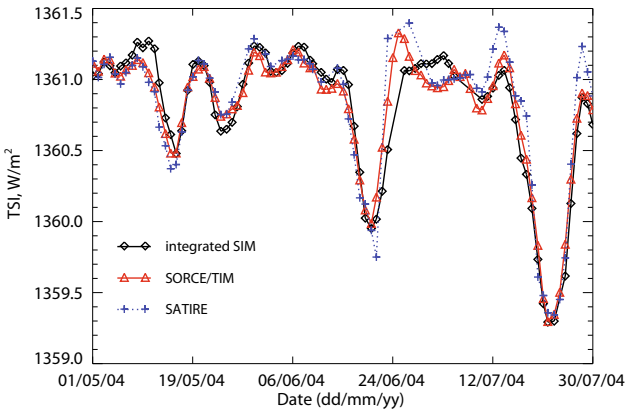

Fig. 3. Total solar irradiance (TSI) from May to July 2004. The black diamonds linked by the solid black lines show the integrated SORCE/SIM data after binomial smoothing; the red triangles show the SORCE/TIM total solar irradiance and the blue plus signs linked by the dotted lines indicate the integrated modelled irradiance. The model and SORCE/SIM data have been integrated between 220 and 1660 nm and have been normalised so that their mean matches the absolute value of the mean SORCE/TIM TSI.

Table 1. Correlation coefficients for the different TSI determinations. The first two columns give the data sets used for the correlations, while the third column lists the Pearson linear correlation coefficient r and its square. The fourth and fifth columns give the more robust Spearman rank correlation, ρ, and its corresponding probability of a chance correlation.

Set 1	Set 2	r [r^2]	ρ	prob
integrated SIM	TIM	0.97 [0.94]	0.86	9×10^{-26}
model	TIM	0.97 [0.94]	0.89	9×10^{-28}
integrated SIM	model	0.92 [0.84]	0.72	1×10^{-20}

1230 W m^{-2}, about 10% lower than the TIM measurements. This value is in reasonably good agreement with model expectations: we find that the model irradiance between 220 and 1660 nm is 1207 W m^{-2}. The comparison between the time dependence of the modelled, SIM integrated and TIM measured irradiance is shown in Fig. 3. Both, the SIM wavelength-integrated data and the modelled TSI were renormalised to match the absolute value of the TIM TSI. For the SIM-integrated TSI, renormalisation should yield an upper limit for the variability amplitude, as the missing part of the spectrum is mainly in the IR where variability levels are expected to be lower. We therefore also tried an approach whereby we added a constant offset. The true behaviour is then expected to lie between these extremes. We found both lightcurves to be very similar with no significant changes for the correlation coefficients, and therefore only present the normalised lightcurves in the following.

The agreement between the SORCE/TIM, integrated SORCE/SIM measurements and the modelled TSI is good overall, as borne out by the correlation coefficients and chance probabilities listed in Table 1 (see Press et al. 1986, for more detail). The difference between the model and the data is of the same order as the difference between the two data sets. Closer inspection of Fig. 3, however, shows that some inconsistencies remain. The model appears least reliable between June 21 and June 30. This is mainly due to a lack of MDI magnetograms and continuum images, and the poorer quality of those magnetograms and images that are available. Furthermore, the model seems to overestimate the facular brightening associated with the spot passage in July. The reason for such an excess brightening could either be that our facular contrast calculations are too high for large active regions, or it could arise through errors in the feature identification, e.g., if some of the spot/pore magnetic flux were wrongly attributed to faculae. This may occur in particular when active regions are near the limb. Finally, uncertainties in the LOS magnetic field correction can lead to the magnetic field strength and hence the contrast of the faculae being overestimated.

Table 2. Central wavelengths and filter widths. For the VIRGO filters largest and smallest wavelength indicate the extent of the *FWHM*. The green and red filters for the model and SIM data are simple rectangular filters.

Filter	VIRGO		SIM/SATIRE	
	λ_c	range	λ_c	range
blue	402.6	400.0–405.3	402.6	400.0–405.3
green	500.9	498.5–503.3	500.0	490.0–510.0
red	863.3	860.5–866.0	865.0	830.0–900.0
red$_S$			775.0	750.0–800.0

The main difference between the integrated SIM data and the other two data sets occurs during the passage of the two small spot groups in May and in the period just after the sunspot passage in June. Compared to either TIM or SATIRE, the integrated SIM data show a larger flux increase before the passage of the first spot group, followed by a stronger flux decrease during the passage of the second spot group. It is not clear what might have led to this difference, as the data do not appear particularly noisy or discontinuous. At the end of June, SIM fails to pick up the facular brightening after the sunspot passage. In fact, the whole period between the two SIM data gaps (around June 24 and July 10) shows a different behaviour than expected from the model or the TIM data. In Sect. 4.2, we show that not all wavelengths are equally affected by this problem. Integration over a bluer wavelength stretch, e.g., one that excludes wavelengths above 800 nm for VIS1, produces a flatter response during that time. The lightcurve is otherwise very similar and the resulting increase in the correlation coefficient is very slight, so that it has not been plotted here.

4.2. Comparisons between SIM, VIRGO and the SATIRE model

Comparisons of VIRGO short-term spectral variations and our model have been presented by Fligge et al. (1998, 2000) and Krivova et al. (2003). Here we extend this work and compare model calculations to SORCE/SIM as well as to the VIRGO/SPM irradiances. The VIRGO/SPM filters are narrow, to the extent that the *FWHM* of the green and red filters lie below the corresponding SIM spectral resolution. The use of a detailed filter profile is meaningless in such a situation and simply employing a single SIM wavelength channel leads to overly noisy narrow-band fluxes. In order to be able to include a larger number of wavelength bands and achieve better signal-to-noise ratios, we used wider, rectangular filters, ranging from 490 to 510 nm in the green, and from 830 to 900 nm in the red. In the blue, we used the VIRGO/SPM bandwidth, as the number of wavelength points covered by the blue filter is significantly larger than in the green and red; furthermore, extending the blue filter is difficult as there is not much clean continuum either side of it. The filter widths and central wavelengths as applied to the different data sets are listed in Table 2.

As discussed in Sect. 3.1.2, the SIM/VIS1 detectors suffer from an imperfectly corrected temperature response above

approximately 820 nm. This proved particularly troublesome in May 2004 and also during the data gap in early July. In order to exclude systematic effects arising through this, we also tested an alternative red channel (red_S, for short red) that was obtained by integrating between 750 and 800 nm. This red_S channel suffers less from temperature-induced variability. Note, however, that the response in the two red channels is different. Our model calculations suggest that the variability in the shorter channel (red_S) should exceed that of the original VIRGO channel by approximately 10%. Comparing the SIM data also suggests a larger response of the shifted red_S channel with respect to the original VIRGO channel (by approximately 6%), though this measurement is uncertain as, on account of the superimposed spurious variability, it has to be determined from a shorter data train.

Comparisons between the VIRGO/SPM data, SIM and our model are shown in Fig. 4. We find that a number of days stand out in all filters. As already found for the TSI, the strongest discrepancy regarding SIM data occurs around June 25, just after the June sunspot passage. SIM apparently fails to pick up the facular brightening as the active region is near the limb; this is particularly salient in the blue and green filters. Note that the red filters mirror some of the problems seen in Sect. 4.1, namely an enhancement in mid May just before the first spot group appears and a rise at the end of June before the data gap. These are even more pronounced in the original red filter (data not shown here) and we thus conclude that they are largely due to an incomplete removal of the instrumental temperature changes that affect the longer wavelength regions particularly strongly.

The largest difference between the model and both SIM and VIRGO data is the much larger facular brightening before and after the July sunspot passage. This is very noticeable in all three filters, as indeed also for the TSI (see Sect. 4.1). By contrast, we find that the sunspot darkening measured by VIRGO and SIM agrees very well with the models, in particular in the green and blue filters; in the red band there is a slight tendency for the darkening to be overestimated. An exception to the good fit is the very small spot at the end of May where the model underestimates the sunspot darkening in all filters.

One way to judge the tightness of the correlation between two data sets is to consider histograms of their fractional differences as shown in Fig. 5. Because of the response problems of SIM/VIS1 for wavelength in excess of about 820 nm, we have used the short red filter (red_S) to obtain the fluxes for the SIM-to-model comparisons. The original central wavelength was used for the model-to-VIRGO comparison and the two different filters are used when comparing VIRGO to SIM. While the number of data points considered here is relatively small, we find that most of the histograms resemble Gaussians, some of them with noticeable skew. The largest deviations are seen for the blue filter for the SIM vs. SATIRE comparison, where the distribution is very broad and may be double-peaked. In most of the cases, however, we can use the width of the standard deviation of a Gaussian fit to the histograms to characterise the scatter between the different data sets. These are listed in Table 3. Note that standard deviations in curved brackets indicate that the histogram had significant skew and/or sidelobes and that a Gaussian was not a good fit.

In order to quantify the fits further, we also list the correlation coefficients in Table 3. To calculate the correlations, we binned the SORCE/SIM and model data onto the same grid as the daily VIRGO/SPM results. Figure 6 shows the correlation plots of the VIRGO/SPM and the SIM filter observations with respect to the model calculations. The dashed blue line indicates a slope of unity as would be expected for a perfect match. The

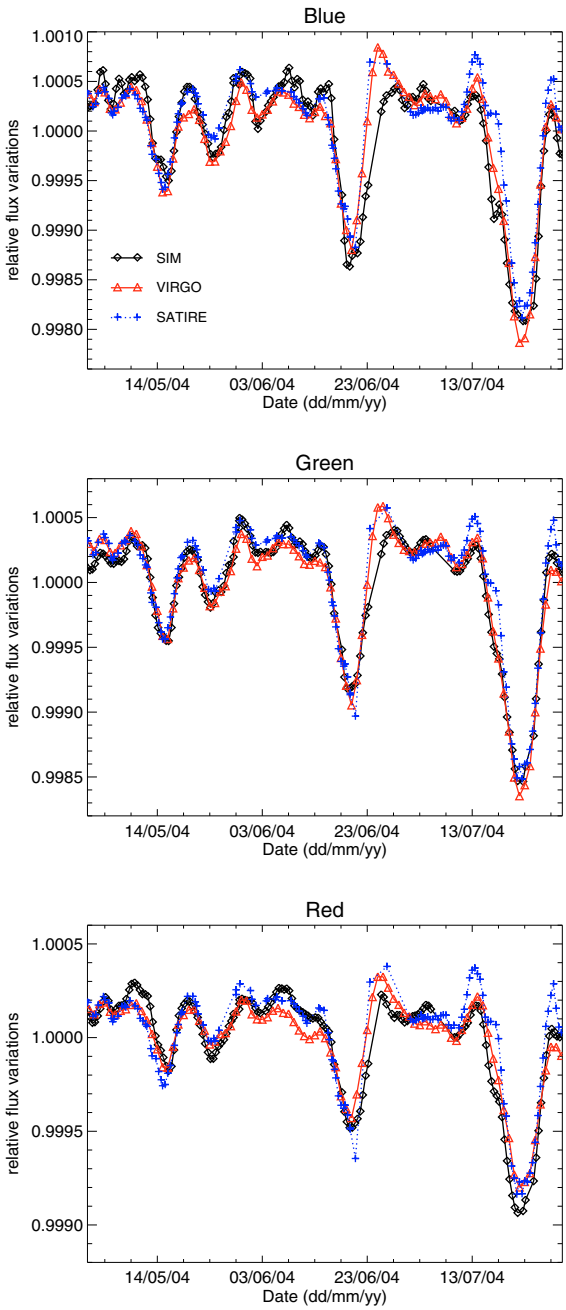

Fig. 4. Comparisons between detrended VIRGO/SPM data (red triangles and lines), and SORCE/SIM (black diamonds) as well as model data (blue plus signs linked by dotted lines) integrated according to the blue, green and red VIRGO filters. In the bottom plot, the SORCE/SIM data are for the red_S filter (see text). Note the different scales for the *y*-axis on the three plots.

red and black lines show the best-fit lines; their slopes are indicated on the graphs and are also listed in Table 3. The slopes were calculated assuming that all data sets suffer from equal relative errors. These errors were estimated from the Gaussian fits to be of the order of 100 ppm in the green and red filter, and of the order of 180 ppm in the blue filter.

When considering all filters together, the correlation coefficients and histogram widths suggest that the best agreement is found between the VIRGO data and SATIRE calculations, while comparisons fare least well for SIM versus SATIRE. The

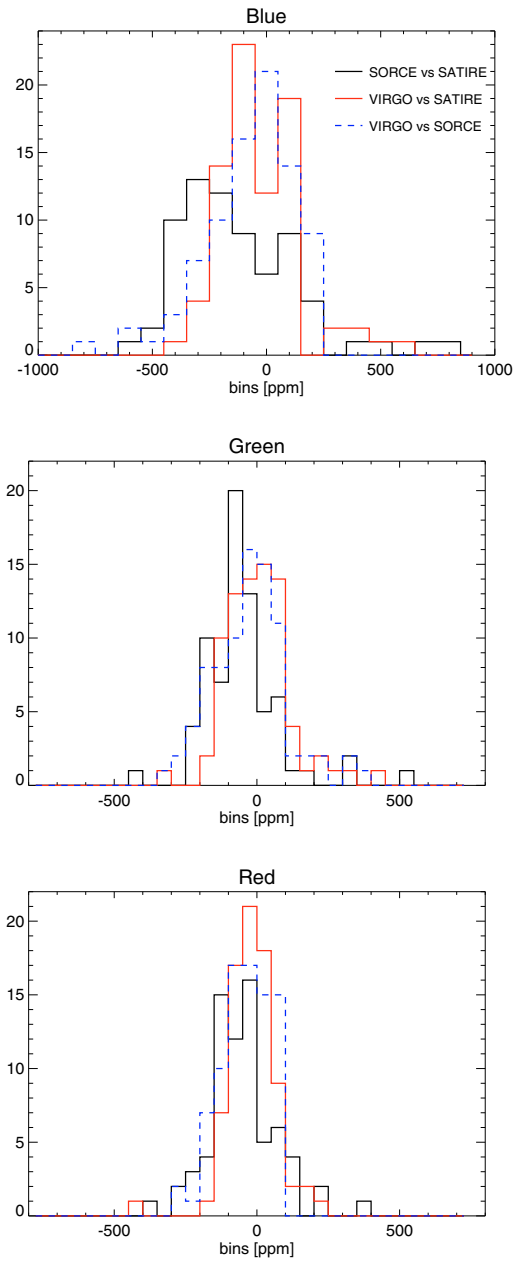

Fig. 5. Histograms illustrating the differences between the measurements and the model in the three VIRGO/SPM channels. The black and red histograms compare SIM, respectively SPM, against SATIRE. The blue dashed lines trace the histograms for SPM vs. SIM. Note that bin widths for the blue filter have been doubled; and that the shorter red_S filter was used for the SIM comparisons.

correlation coefficients and plots indicate that the agreement between the model and the observations is best for the green filter, but slightly less good for both the red and blue filters. In the following, we discuss the fits for the individual filters in more detail.

The correlation coefficients in the red filter show a relatively large variation, ranging from a tight correlation with coefficient 0.96 (r^2 = 0.90) between VIRGO data and model calculations, down to a coefficient of 0.77 (r^2 = 0.59) for SIM/red to model comparisons. This latter value can largely be explained

Table 3. Table listing the standard deviation in ppm (σ_i) derived from gaussian fits to the histograms shown in Fig. 5, the linear correlation coefficient (r_i), its square, and the regression slope (m_i) in the three VIRGO/SPM filters. VIR, SOR and SAT indicate VIRGO/SPM data, SORCE/SIM data and the SATIRE model, respectively. In the rows with the regression slopes, the square brackets give the errors on the slopes, assuming equal errors for SIM, VIRGO/SPM and SATIRE. As there are no VIRGO data for the red_S filter, Cols. 2 and 3 in the last three lines are for comparisons between the standard VIRGO red band and the SIM and SATIRE red_S bands.

Parameter	VIR vs. SOR	VIR vs. SAT	SOR vs. SAT
N	84	79	71
σ_blue	172	146	(231)
r_blue, $[r^2_\text{blue}]$	0.95 [0.90]	0.96 [0.92]	0.89 [0.79]
m_blue	0.93 [0.04]	1.10 [0.05]	1.18 [0.06]
σ_green	109	95	92
r_green, $[r^2_\text{green}]$	0.98 [0.96]	0.97 [0.95]	0.96 [0.92]
m_green	1.04 [0.04]	1.04 [0.03]	0.99 [0.04]
σ_red	(85)	71	(177)
r_red, $[r^2_\text{red}]$	0.89 [0.78]	0.95 [0.90]	0.77 [0.59]
m_red	0.69 [0.04]	0.88 [0.06]	...
$\sigma_\text{red,s}$	93	...	91
$r_\text{red,s}$, $[r^2_\text{red,s}]$	0.96 [0.92]	0.96 [0.91]	0.92 [0.84]
$m_\text{red,s}$	0.82 [0.05]	...	0.95 [0.06]

by the temperature-induced sensitivity problems for SIM/VIS1 above about 850 nm. A comparison between the model and SIM data for the slightly shorter red_S filter where this is less of an issue gives a significantly higher correlation coefficient of 0.92 (r^2 = 0.84). Despite the filter shift and the associated change in responsivity to spot and facular passages, there is also an increase in the correlation coefficient (from 0.89 to 0.96) when comparing VIRGO red with SIM/red_S.

In terms of the correlation coefficient, there is no significant difference between using the model calculations for the red or red_S filter to compare with a given observed time series. This is expected, as the basic features of the model differ only very slightly between the two wavelength bands. The amplitude of the variability, however, matches much better when the model calculations are carried out for the filter appropriate for the comparison data.

The slopes derived for the red correlations show that SATIRE overestimates the amplitude of the variability by about 5% (SORCE/SIM) and 10% (VIRGO). For the SIM analysis, we used the alternative "short" red filter as this is essentially unaffected by the temperature effects. Note that the very small gradient of 0.88 derived for the VIRGO vs. model comparisons is in part due to a single outlying model point on June 21, shown as the red triangle at (0.99935, 0.99975) in the bottom plot of Fig. 6 (see also Fig. 4). If this outlier is excluded, the gradient increases to 0.91 which is in better agreement with the results for SIM. A further reason for the low gradient could be that the red filter band includes the redmost line of the Ca II IR triplet that might not be modelled well by SATIRE.

The correlations between all the data sets are excellent in the green filter. In fact, they are better than those determined for the TSI comparisons, presumably because they are limited to the similar narrow spectral region and therefore sample a well-definied region of the solar atmosphere. We also find that the gradients of the best-fit lines are near unity, indicating that the amplitude of the variability agrees between all three datasets. In the blue filter, the agreement between the model calculations and

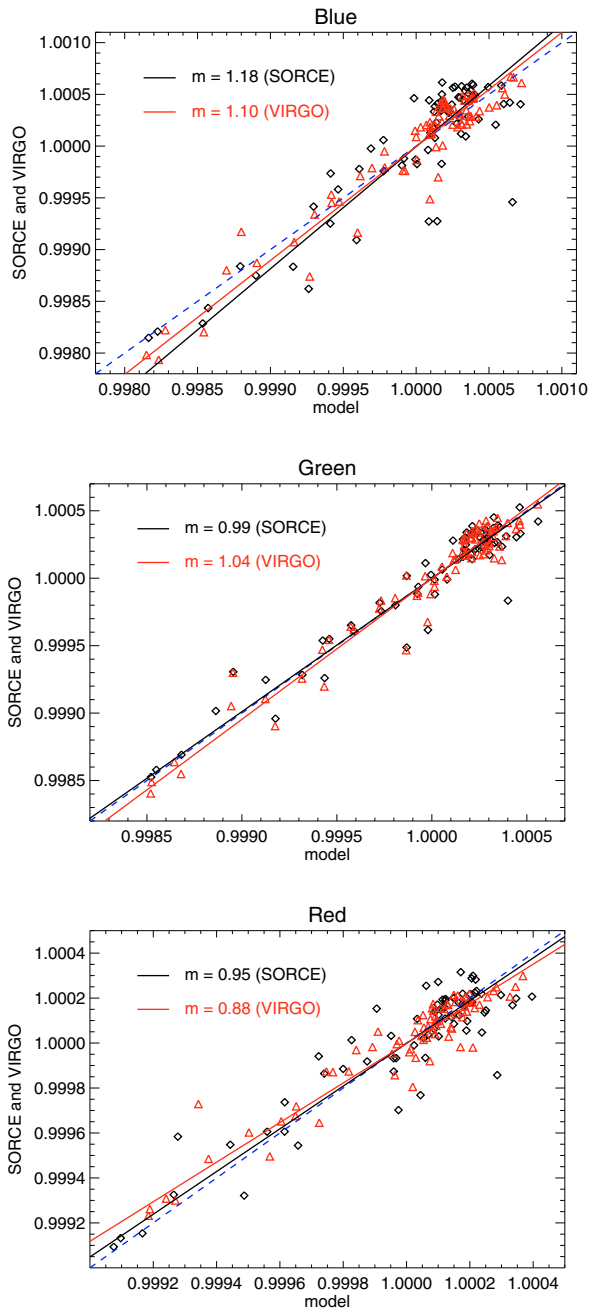

Fig. 6. Plots of VIRGO/SPM and SORCE/SIM vs. SATIRE in the blue (*top*), green (*middle*) and red (*bottom*) VIRGO channels. The black diamonds are for SIM vs. model, the red triangles for VIRGO vs. model data. The blue thin dashed line indicates a unit gradient, while the solid black and red lines show the gradients for the best linear fits for the SIM and VIRGO data, respectively.

VIRGO is comparable to that of the TSI comparisons, though the model fares less well with respect to the SIM data. As indicated by the correlation gradients, the model appears to underestimate the variability by between 10 and 20%. We consider the 20% derived from SIM data to be less reliable, mainly because the data follow a slight degradation-like long-term trend. This is again most obvious at the beginning of May. A correlation analysis with data after May 11 yields a slope of 1.11 with respect to the model, and agrees well with our findings for the blue VIRGO filter.

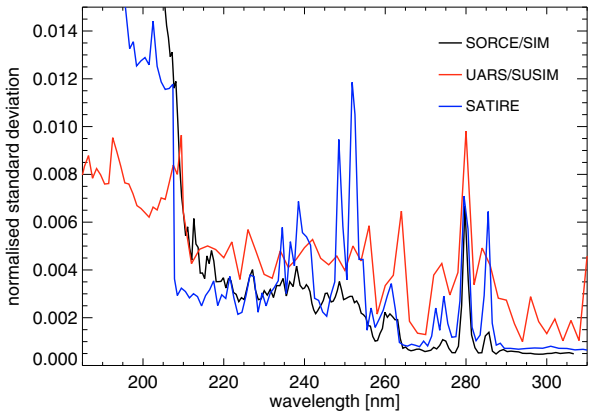

Fig. 7. Normalised standard deviation for SORCE/SIM (black line), UARS/SUSIM (red) and the SATIRE model (blue) calculations. To lessen the confusion of the plot, the SIM data have been wavelength binned by factors of 10 and 5 below and above 240 nm respectively; the SUSIM data were binned by a factor of two for wavelengths above 210 nm.

4.3. Comparisons between SIM, SUSIM and the SATIRE model

During 2004, the solar UV spectrum and its variability was also recorded with the UARS/SUSIM instrument. In this section, we compare these measurements with the SORCE/SIM measurements and the model calculations for wavelengths between 170 and 320 nm. Figure 7 shows a plot of the normalised standard deviation for data and model calculations between May 1 and July 31 in 2004. In order to reduce confusion in the plot, we have binned the SORCE/SIM and UARS/SUSIM data in the wavelength domain before carrying out the variability analysis. The binning factors are detailed in the caption of Fig. 7. A number of striking features are apparent in the plot, and are discussed below.

The SORCE/SIM and SATIRE data show a large increase in variability at about 205 nm. This is most likely due to Al and Ca opacity edges between 200 and 210 nm. A significant decrease of the solar brightness temperature around this wavelength was already observed by Widing et al. (1970) based on data from rocket flights. It is very noticeable, however, that the variability recorded by UARS/SUSIM is much lower than both the SORCE/SIM and the SATIRE variability. While the UARS/SUSIM increase might appear weakened because of the higher (instrumental) variability seen above 200 nm and the lower velocity resolution, we expect the SUSIM data to best reflect the solar variability below 200 nm during the time period considered here. The main reason for the (excessive) increase in variability of the SATIRE model is the breakdown of the LTE assumptions and the use of opacity distribution functions (ODFs) rather than detailed line-opacity calculations. In the case of SIM, the jump in variability is not surprising either, as its detector is not expected to perform well at these wavelengths (see Sect. 3.1.1). Better results should be provided by SORCE/SOLSTICE.

In the wavelength region between 210 and 290 nm, the agreement between the model calculations and the SIM measurements is varied. While some features such as the Mg II h&k lines (280 nm), and the regions from 220 to 232 nm, from 255 to 270 and above 290 nm match well, other wavelength regions show large disagreements, see, e.g., the lines of Mg I at 285 nm, or the complex sets of lines around 240 and 250 nm. As above, these disagreements are due mainly to the

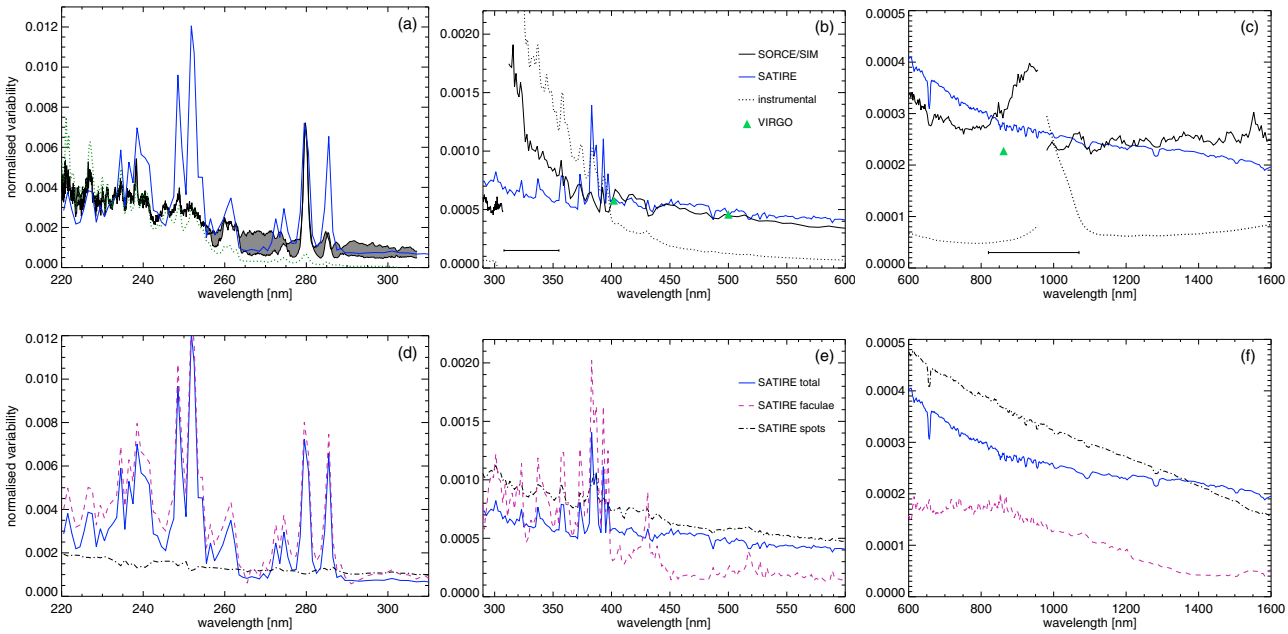

Fig. 8. Normalised standard deviation over the whole SORCE/SIM wavelength region. *From left to right*, the panels show the variability between 220 and 320 nm, between 290 and 600 nm and between 600 and 1600 nm. The top figures show the modelled and the observed variability in blue and black, respectively; in the left-most plot, the grey-shaded area indicates the range of variability for SIM, depending on whether a linear trend is removed. Also shown is the instrumental noise limit (dotted lines) and the variability measured in the three VIRGO filters (green triangles). The horizontal solid lines offset from the plots indicate the wavelength ranges where instrumental noise and artefacts dominate the variability. The bottom plots show the modelled variability, distinguishing between total variability (blue solid line), the spot (dotted black) and facular (dashed purple) contributions.

assumption of LTE and the use of ODFs (Kurucz 1992). Uncertainties in the model atmospheres also contribute, though probably to a much smaller extent, since the differences are largest at the wavelengths of strong lines showing strong NLTE effects. Thus the difference in the behaviour of the Mg I and Mg II resonance lines can be explained quite well if NLTE effects are taken into account (Uitenbroek & Briand 1995).

Overall, the agreement between SIM and SUSIM is reasonably good between about 210 and 290 nm. While the variability recorded with SUSIM is higher due to its lower sensitivity, the features recovered agree well and the measured relative variabilities are not too different. Above 290 nm UARS/SUSIM shows a relatively poor response that swamps the solar variability on mid to short-term time scales. The responsivity and noise characteristics of SUSIM have been well documented and are discussed, e.g., in Woods et al. (1996).

4.4. Comparison of SIM with the SATIRE model over the whole wavelength range

The main advantage of SIM over the VIRGO/SPM channels is that a much more complete sampling of wavelengths is available. Figure 8 shows the rms variability between May and August 2004 over the whole analysed SORCE/SIM wavelength range. The normalised standard deviation of the SORCE/SIM data is indicated by the solid black lines in panels a to c, though note that the grey-shaded area on panel a indicates the range in variability that is obtained depending on whether a linear trend is removed from the data or not. The horizontal bars in Figs. 8b and c indicate the wavelength regions where the measured variability is dominated by instrumental noise (black dotted lines). The modelled variability is indicated by the blue lines. The bottom plots (d, e and f) show the contributions of the spots (dotted black lines) and faculae (dashed purple lines) to the overall variability. To calculate these, we replaced the facular (resp. sunspot) contribution by a quiet-Sun contribution. The curves show very clearly that the wavelength dependence of spot variability is spectrally much smoother than the facular variability. This has to do with the fact that the darkening due to spots is dominated by the drop in continuum intensity. Changes in spectral lines produced by the lower temperature in spot umbrae and penumbrae play a secondary role. For faculae, the absolute temperature difference is less pronounced (especially in the lower atmosphere), and it is the different temperature gradient that produces changes in the continuum as well as in the lines. Especially at shorter wavelengths, individual and groups of lines provide the dominant contribution (Mitchell & Livingston 1991; Unruh et al. 2000).

Below about 280 nm, the variability due to faculae generally exceeds that due to spots; then follows a region up to 400 nm where they are mostly of comparable magnitude. Above 400 nm, the modelled spot variability is always larger than the facular variability, and the combined variability follows the spot variability closely. Note that there is a further cross-over around 1.4 μm where the modelled variability of the spots and faculae drops below the total variability. This marks the transition where the facular model becomes dark averaged over the solar disk and thus no longer acts to counterbalance the spots. The fact that the model shows a smaller variability than SIM at these wavelengths cannot be due to this property of the model; dark faculae enhance the darkening due to spots, and thus increase the standard deviation (see also Sect. 5). In other words, if the model faculae were bright at these wavelengths the discrepancy between the SATIRE model and SIM data would be larger.

The shift in importance away from faculae to spots at wavelengths as low as about 300 nm is expected when considering variability on the order of a couple of month, i.e., on the

Table 4. Table listing the different bands used to calculate the time series. The first column gives the label as used for the plots, the second and third columns give the start and end wavelengths for the bands, while column four gives the number of flux points over which the integral was carried out for the SORCE/SIM data. Columns 5 and 6 give the mean fluxes for each band as derived from the SIM measurements and the model calculations. The last three columns list the correlation coefficients, the gradient and the y-axis flux offsets of a linear fit of the data to the model; the gradient and offset for Ca II is in brackets as the correlation coefficient is rather low.

Band	λ_S	λ_E	Number of	Flux (data)	Flux (model)	Correlation	Gradient	Offset
	[nm]	[nm]	flux points	[W m^{-2}]	[W m^{-2}]	coef	(vs. model)	
[1]	[2]	[3]	[4]	[5]	[6]	[7]	[8]	[9]
230	220	240	271	1.02	0.98	0.90	0.99	0.06
Mg II h&k	277	283	38	1.20	0.71	0.96	1.03	0.47
Ca II H&K	391	398	14	7.21	5.60	0.51	(0.95)	(1.89)
G-band	420	435	22	23.5	21.3	0.77	1.35	–5.3
511	507	516	7	13.5	15.3	0.95	0.88	0.1
Hα	644	668	10	32.0	33.8	0.96	0.84	3.6
1065	1050	1080	6	16.7	15.8	0.89	1.24	–2.9
1550	1527	1583	10	12.9	14.6	0.93	1.33	–6.4

rotation time scale when the influence of spots tends to dominate the TSI. On longer time scales such as that of the solar cycle, however, bright small-scale magnetic features dominate the TSI variations, and are thus also expected to dominate variability in both the UV and visible.

4.5. SIM & SATIRE time series

In this section, we compare the variability in a number of wavelength bands in more detail. The wavelength bands have been picked so as to show the change in behaviour going from the UV around 220 nm, up to the IR at 1.5 μm. They are typically also chosen at wavelengths where the relative variability is high and the data quality is good. The wavelength bands are listed in Table 4, along with their band widths and the number of data points included in the integration of the SIM data. So as to improve the S/N level of the resulting time series, the UV bands, in particular, have been chosen to include a large number of wavelength points. Note that the noise level of the modelled time series is largely governed by the noise in the magnetograms and cannot be decreased by increasing the number of wavelength points considered; the absolute flux level, however, is influenced by the coarseness of the wavelength grid.

The measured and modelled timeseries are shown in Figs. 9 and 10 and the correlation coefficients as well as the slopes between the model and the data are listed in Table 4. The upper panels show the measured and modelled solar variability while the bottom panels show the modelled contributions of the faculae and spots to the irradiance variations. The figures illustrate again the rapid decrease in the variability towards longer wavelengths. Additionally, they show the change in the lightcurve aspects as one moves from the UV to the visible. In the UV, as illustrated by the 230 and 280 nm bands (Fig. 9), the influence of the spots is so small that their darkening effect is more than compensated for by the faculae, even on solar rotational time scales. Furthermore, the facular contrast increase towards the limb is not sufficient at these wavelengths to counteract the projection effects. Consequently, the Sun appears brightest when the main spot groups are nearly at disk centre.

At our resolution, this behaviour is no longer observed at longer wavelengths, such as in the Ca II and the G bands. The spot darkening is now sufficient to offset the facular brightening, at least when the active regions are near disk centre. The overall lightcurves thus appear somewhat confusing, with rapid sequences of peaks and dips, and very few stretches of "quiet"-Sun behaviour. Further high-resolution calculations would be required to check whether this behaviour also holds for the individual line cores, or whether we are currently seeing a mix of line and continuum behaviour. The low wavelength resolution of the model and the failure to calculate exact line profiles partly explains the relatively large difference in the observed and modelled mean flux in the Mg II and, in particular, 395 nm (Ca H&K) bands, where the model only includes 4 wavelength points. A further reason for the difference in flux is due to our assumption of LTE, most markedly for Ca H&K.

The situation again changes when looking at (continuum) bands and longer wavelengths in general (see left-hand panel in Fig. 10). The facular brightenings are now much weaker and mostly show a double-peaked aspect, i.e., the faculae produce most of the brightening when near the limb, and very little or even no brightening when at disk centre. Combined with the spot contribution, this leads to the familiar spot-dominated light curves, with small brightenings just before and after spot passages. Such behaviour is indeed seen for the TSI, and has been discussed at length in the previous section.

In the NIR, finally, the facular brightenings become very weak, and might even disappear completely for the facular model atmosphere we employ. This is suggested by the model calculations for the 1550 nm band that differ markedly from those for the 1065 nm band. Figure 10 suggests that the spots are not sufficiently dark at 1550 nm and indicates that the temperature of the spot model atmosphere is too high in the deeper layers (1550 nm is close to the opacity minimum and thus carries information on the deepest observed layers). But while the model calculations appear to underestimate the flux decrease due to most of the active regions, they agree very well with the timing of the flux decrease; note that the dips due to the spot passages are significantly wider at 1.55 than at 1.07 μm in the observed as well as in the modelled data. In the model, the wider spot passages are a consequence of the very small contrast of the faculae at that wavelength. Figure 11 shows a comparison of the model facular contrast for the six longer wavelength bands. The contrast at 1550 nm shows the lowest values throughout and becomes negative near the disk centre ($\mu > 0.5$). This low contrast means that only very little facular brightening is seen near the limb and thus leads to an earlier onset of the spot-induced darkening, as illustrated on the right-hand plots of Fig. 10.

We note that at 1.55 μm, there is rather poor agreement between the model calculations and the SIM data during May 2004. In particular, we find that the SIM data show a reversal in the relative spot strength during May. The first spot (centred around May 15th) is significantly stronger than the spot

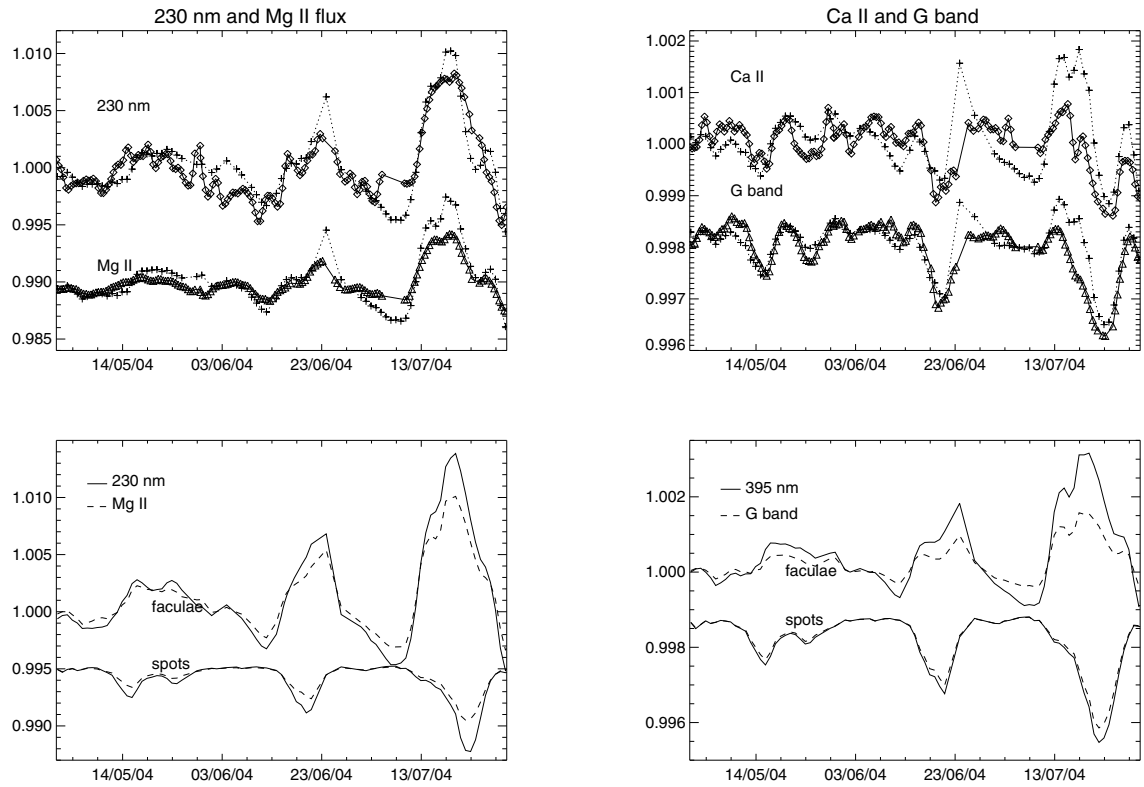

Fig. 9. *Top plots*: flux variations for the 230 nm and the Mg II band (*left-hand side*) and for the 395 nm and the G band (*right-hand side*). The exact band widths are listed in Table 4. The diamonds linked by the solid lines represent SIM data, the plus signs and dotted lines show the model calculations. Note that the modelled timeseries have been binned onto daily values; the SIM data remain on their original time resolution, but have been smoothed using a binomial filter. *Bottom plots*: modelled time series for the facular and spot contributions. The upper lines are for the faculae, the lower for the spots. The band wavelengths for the solid and dashed lines are indicated on the plots.

at the end of May in all wavebands, except at 1.55 μm, where the second spot appears darker. This could indicate that the temperature gradient in the two spots is different, although we cannot exclude uncorrected data fluctuations.

5. Discussion and conclusions

We have presented and compared SATIRE model calculations and measurements of spectral solar variability on rotational time scales. The data and calculations cover a 3-month time span from May to July 2004. In addition, we also compare modelled and observed time series of the total irradiance variability and the variability in a number of selected wavelength bands. Such comparisons are particularly timely as SORCE/SIM is able to provide unprecedented observations over most of the range starting in the UV at approximately 220 nm and including the visible as well as the near infrared up to 1.6 μm.

We find excellent agreement between the modelled total solar irradiance variations and the SORCE/TIM measurements. The absolute value of the wavelength-integrated SORCE/SIM measurements is in line with the expected model fluxes, and its variability agrees well except on a small number of days when the data quality was poorer (see Fig. 3). We find correlation coefficients of 0.97 and 0.92 when comparing the modelled total solar irradiance with TIM and the wavelength integrated SIM measurements, respectively.

The modelled and measured spectral variability over the three months is summarised in Fig. 8 for wavelengths between 220 and 1600 nm. Overall, we find good agreement between the model and the observations. Agreement is particularly good between 400 and 1300 nm. In the UV, where we also compare the SIM measurements to UARS/SUSIM, the agreement is somewhat patchy; some strong individual lines, such as the Mg II h&k doublet, match very well, others, such as Mg I and Ca II H&K, agree only poorly. This is not too surprising as we use opacity distribution and assume LTE throughout. Uitenbroek & Briand (1995) have shown that NLTE effects can explain much of the different behaviour of the Mg I and Mg II resonance lines. We also note that the resolution of our calculations is insufficient to resolve even the strong lines and to capture their complex behaviour. The role of spectral resolution in the context of line variability has been discussed, e.g., in White et al. (2000).

In the wavelength range between approximately 310 nm and 350 nm, possibly even up to 390 nm, the response of both SORCE/SIM and UARS/SUSIM is too poor to determine solar variability on the rotational time scale. The best estimate of variability at those wavelengths is currently provided by the SATIRE model. The model calculations allow us to isolate the facular and spot contribution. This, together with the light-curves, illustrates very clearly the change from facular dominated variability at short wavelengths to spot-dominated variability above approximately 400 nm.

In the visible, the observed and modelled irradiance variability matches well, though the decrease in the variability at longer wavelengths appears somewhat steep in the model compared to the observations. We find, e.g., that the SATIRE model overestimates the variability between about 600 and 800 nm by up to 20% compared to the SIM measurements, while it

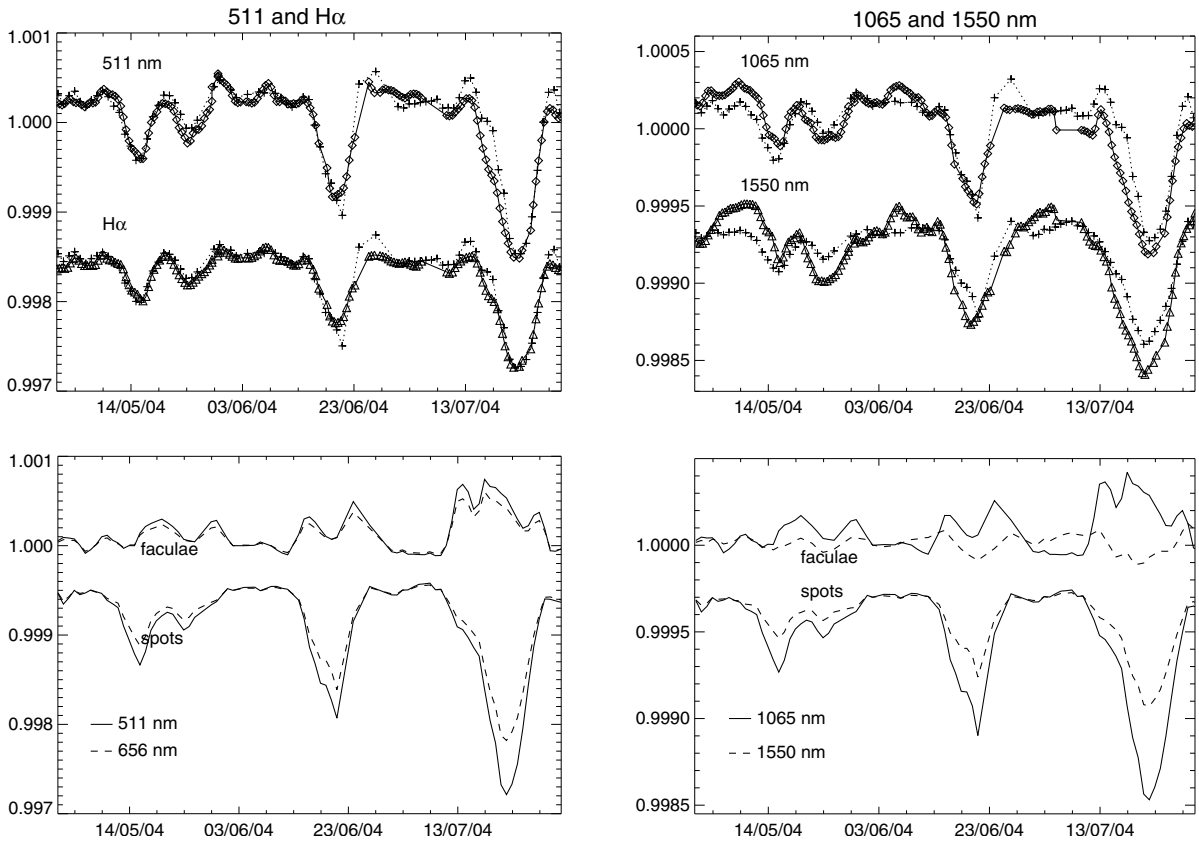

Fig. 10. Same as Fig. 9, though this time showing wavelength bands centred at 511 nm and at Hα respectively (*left-hand side*), and two near-IR bands centred at 1065 and 1550 nm, respectively (*right-hand panels*).

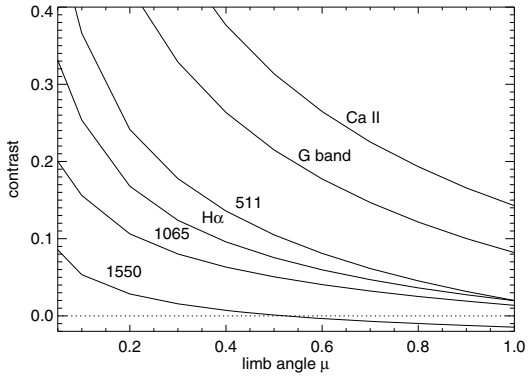

Fig. 11. A plot of the modelled contrasts in the 6 longer wavelength bands from Table 4. The contrast decreases very strongly with wavelength, becoming negative at the disk centre at the near IR, as illustrated by the bottom curve for 1550 nm. The contrasts in the Mg II and 230 nm bands are much higher and are not plotted here. Note also that these contrasts are maximum values that are scaled by the facular filling factors.

underestimates the variability around 1.5 μm by a similar amount. Note that for wavelengths between 800 and 1000 nm, the SIM detectors suffer from temperature-induced variability that cannot yet be fully compensated for; we were therefore unable to carry out meaningful comparisons at those wavelengths. As a cross-check, we further compared the SATIRE and SORCE/SIM variability with the VIRGO/SPM measurements at 400, 500 and 860 nm. We found that the correlation coefficients for the model-to-data comparisons are typically very similar to those obtained for the SPM-to-SIM data comparisons.

Our model suggests that the overall effect of faculae at 1.6 μm is one of darkening, though they appear bright at all wavelengths when seen close to the limb. Near 1.6 μm, the small brightness enhancement seen for faculae at the limb, however, is typically offset by the spots, so that active-region passages produce longer-lasting brightness dips at this wavelength than at shorter wavelengths. This is illustrated on the right-hand panel of Fig. 10. Contrary to Fontenla et al. (2004), we find no evidence for overall bright faculae during the comparatively quiet period analysed here. An unambiguous contrast determination is difficult, however, as most large facular regions tend to be accompanied by dark spots whose exact contrasts are also unknown.

Acknowledgements. The authors would like to thank L. Floyd for helpful discussions and information on SUSIM data, M. Snow for information on the SORCE/SOLSTICE data and C. Fröhlich for his comments on the paper and help with the VIRGO/SPM data. This work was supported by the *Deutsche Forschungsgemeinschaft, DFG* project number SO 711/1-1 and by the NERC SolCli consortium grant.

References

Brueckner, G. E., Edlow, K. L., Floyd, L. E., Lean, J. L., & Vanhoosier, M. E. 1993, J. Geophys. Res., 98, 10695
Dewitte, S., Crommelynck, D., & Joukoff, A. 2004, J. Geophys. Res. Space Phys., 109, 2102
Fligge, M., Solanki, S. K., Unruh, Y. C., Fröhlich, C., & Wehrli, C. 1998, A&A, 335, 709
Fligge, M., Solanki, S. K., & Unruh, Y. C. 2000, A&A, 353, 380
Floyd, L. E., Herring, L. C., Prinz, D. K., & Crane, P. C. 1998, in Optical Systems Contamination and Degradation, Proc. SPIE, 3427, 445

Floyd, L., Rottman, G., DeLand, M., & Pap, J. 2003a, ESA SP, 535, 195
Floyd, L. E., Cook, J. W., Herring, L. C., & Crane, P. C. 2003b, Adv. Sp. Res., 31, 2111
Fontenla, J., White, O. R., Fox, P. A., Avrett, E. H., & Kurucz, R. L. 1999, ApJ, 518, 480
Fontenla, J. M., Harder, J., Rottman, G., et al. 2004, ApJ, 605, L85
Fröhlich, C., & Lean, J. 1998, Geophys. Res. Lett., 25, 4377
Fröhlich, C., Romero, J., Roth, H., et al. 1995, Sol. Phys., 162, 101
Fröhlich, C., Crommelynck, D., Wehrli, C., et al. 1997, Sol. Phys., 175, 267
Harder, J., Lawrence, G., Fontenla, J., Rottman, G., & Woods, T. 2005a, Sol. Phys., 230, 141
Harder, J. W., Fontenla, J., Lawrence, G., Woods, T., & Rottman, G. 2005b, Sol. Phys., 230, 169
Kopp, G., & Lawrence, G. 2005, Sol. Phys., 230, 91
Kopp, G., Lawrence, G., & Rottman, G. 2005, Sol. Phys., 230, 129
Krivova, N. A., Solanki, S. K., Fligge, M., & Unruh, Y. C. 2003, A&A, 399, L1
Krivova, N. A., Solanki, S. K., & Floyd, L. 2006, A&A, 452, 631
Kurucz, R. L. 1992, Rev. Mex. Astron. Astrofis., 23, 181
Kurucz, R. L. 1993, CDROM # 13 (ATLAS9 atmospheric models) and # 18 (ATLAS9 and SYNTHE routines, spectral line database), Tech. rep. (Cambridge, MA: Harvard-Smithsonian Center for Astrophysics)
Lean, J. 1989, Science, 244, 197
Lean, J., Rottman, G., Harder, J., & Kopp, G. 2005, Sol. Phys., 230, 27
Marchand, P., & Marmet, L. 1983, Rev. Sci. Instr., 54, 1034
Mitchell, W. E. J., & Livingston, W. C. 1991, ApJ, 372, 336
Ortiz, A., Solanki, S. K., Domingo, V., Fligge, M., & Sanahuja, B. 2002, A&A, 388, 1036
Press, W. H., Flannery, B. P., Teukolsky, S. A., & Vetterling, W. T. 1986, Numerical Recipes: The Art of Scientific Computing (Cambridge: Cambridge University Press)
Prinz, D. K., Floyd, L. E., Herring, L. C., & Brueckner, G. E. 1996, in Ultraviolet Atmospheric and Space Remote Sensing: Methods and Instrumentation, Proc. SPIE, 2831, 25
Rottman, G., Harder, J., Fontenla, J., et al. 2005, Sol. Phys., 230, 205
Skupin, J., Noël, S., Wuttke, M. W., et al. 2005, Adv. Sp. Res., 35, 370
Snow, M., McClintock, W. E., Rottman, G., & Woods, T. N. 2005, Sol. Phys., 230, 295
Solanki, S. K., & Stenflo, J. O. 1984, A&A, 140, 185
Solanki, S. K., & Brigljević, V. 1992, A&A, 262, L29
Uitenbroek, H., & Briand, C. 1995, ApJ, 447, 453
Unruh, Y. C., Solanki, S. K., & Fligge, M. 1999, A&A, 345, 635
Unruh, Y. C., Solanki, S. K., & Fligge, M. 2000, Space Sci. Rev., 94, 145
Wenzler, T., Solanki, S. K., Krivova, N. A., & Fröhlich, C. 2006, A&A, 460, 583
White, O. R., Fontenla, J., & Fox, P. A. 2000, Space Sci. Rev., 94, 67
Widing, K. G., Purcell, J. D., & Sandlin, G. D. 1970, Sol. Phys., 12, 52
Willson, R. C., & Hudson, H. S. 1988, Nature, 332, 810
Willson, R. C., & Mordvinov, A. V. 2003, Geophys. Res. Lett., 30, 3
Woods, T. 2007, SORCE Newsletter, ed. V. George (Colorado: LASP)
Woods, T. N., Prinz, D. K., Rottman, G. J., & et al. 1996, J. Geophys. Res., 101 (D6), 9541